Silesian University of Technology

ECOS 2019

Proceedings of the

32nd International Conference on Efficiency, Cost, Optimization, Simulation and Environmental Impact of Energy Systems

Edited by
Wojciech Stanek, Paweł Gładysz, Sebastian Werle, Wojciech Adamczyk

Wrocław, Poland, 23-28 June 2019

Wrocław University of Science and Technology

Edited by Wojciech Stanek, Paweł Gładysz, Sebastian Werle, Wojciech Adamczyk

Proceedings of the

32nd International Conference

on Efficiency, Cost, Optimization, Simulation and Environmental Impact of Energy Systems

Wrocław, Poland, 23-28 June 2019

Scientific Editors: Wojciech Stanek, Paweł Gładysz, Sebastian Werle, Wojciech Adamczyk

Technical Editors: Lucyna Czarnowska, Tomasz Simla, Tomasz Krysiński

Cover design: Lucyna Czarnowska, Karolina Petela

Second edition

ISBN 978-83-61506-51-5

Published by Institute of Thermal Technology

Available: http://www.s-conferences.eu/ecos2019

Preface

On behalf of the Organizing Committee, it is the greatest pleasure to welcome you to ECOS 2019 - the 32nd International Conference on Efficiency, Cost, Optimization, Simulation and Environmental Impact of Energy Systems that has been organized for the third time in Poland. This year we meet in Wroclaw - the historical capital city of Silesia and Lower Silesia, and the host of the European Capital of Culture in 2016. So far, the following editions of ECOS conference took place in Poland:

1. 1993, July 5-9, Cracow, Poland: Energy Systems and Ecology (ENSEC ´93), International Conference, Chairmen: J. Szargut, G. Tsatsaronis, Z. Kolenda, A. Ziębik.
2. 2008, June 24-28, Cracow-Gliwice, Poland: The 21st International Conference on Efficiency, Costs, Optimization, Simulation and Environmental Impact of Energy Systems (ECOS 2008), Chairmen: Andrzej Ziębik, Zygmunt Kolenda, Wojciech Stanek.

ECOS 2019 continues the tradition of bringing together distinguished scientists, engineers and professionals as an outstanding international community of experts in the domain of energy systems. It is an honour for us to host such a distinguished community whose excellence has been, for the last three decades, at the forefront of energy systems development. All participants of the conference have the possibility to disseminate their work, to share and exchange opinions and knowledge within the sessions planned for ECOS 2019. We wish you the fruitful discussions and negotiations during the stay in Wrocław. The conference would not be possible without all the excellent papers contributed by the authors, as well as by the outstanding invited lecturers. We would like to thank all the authors for their contributions and their participation in ECOS 2019.

Prof. Wojciech Stanek
ECOS 2019 Chairman
Silesian University of Technology, Gliwice, POLAND

Prof. Zbigniew GNUTEK
Prof. Sławomir PIETROWICZ
ECOS 2019 Co-chairmen
Wroclaw University of Science and Technology, POLAND

and All Organizing Committee

Organizing committee

Silesian University of Technology
Institute of Thermal Technology
Gliwice, Poland

Professor Wojciech STANEK
Chair of the Conference

Dr. **Lucyna CZARNOWSKA**
Dr. **Paweł GŁADYSZ**
Assoc. Prof. **Sebastian WERLE**
Assoc. Prof. **Wojciech ADAMCZYK**
MSc **Karolina PETELA**
MSc **Krzysztof PAJĄCZEK**
MSc **Tomasz SIMLA**
Dr. **Tomasz KRYSIŃSKI**
MSc **Bartłomiej RUTCZYK**

Administrative specialist

MSc **Justyna JANIK VIDEIRA**
MSc **Joanna SŁOWIK**

Conference system

MSc **Wojciech LITWIN**

Wroclaw University of Science and Technology
Faculty of Mechanical and Power Engineering
Wroclaw, Poland

Professor Zbigniew GNUTEK
Co-chair of the Conference

Assoc. Prof. Sławomir PIETROWICZ
Co-chair of the Conference

MSc **Agnieszka OCHMAN**
MSc **Maciej CHOLEWIŃSKI**
Dr. **Katarzyna STRZELECKA**

Administrative specialist

MSc **Barbara KARCZ**

Honorary chairs

Professor Andrzej ZIĘBIK
Silesian University of Technology
Professor Zygmunt KOLENDA
AGH University of Science and Technology

Scientific committee

Abel Hernandez-Guerrero
Alberto Mirandola
Alojz Poredoš
Ana M Blanco Marigorta
Andrea Lazzaretto
Andrej Kitanovski
Andrzej Ziębik
Anna Stoppato
Antonio Valero
Asfaw Beyene
Brian Elmegaard
Carlos Pinho
Christos A. Frangopoulos
Daniel Favrat
Edson Bazzo
Enrico Sciubba
Erwin Franquet
Francois Marechal
George Tsatsaronis
Giampaolo Manfrida
Gordana Stefanović
Guangming Chen
Henrik Lund
Honguang Jin
Jean-Pierre Bedecarrats
José Carlos Teixeira
Lucyna Czarnowska
Mauro Reini
Michael Moran
Michael Von Spakovsky
Michel Feidt
Na Zhang
Noam Lior
Ofira Ayalon
Ozer Arnas
Pascal Stouffs
Paweł Gładysz
Peter Rae
Rene Cornelissen
Richard Gaggioli
Ron Zevenhoven
Ryohei Yokoyama
Sebastian Werle
Senhorinha Teixeira
Signe Kjelstrup
Silvia Nebra
Silvio de Oliveira Júnior
Soteris Kalogirou
Sotirios Karellas
Sylvain Quoilin
Tatiana Morosuk
Umberto Desideri
Vittorio Verda
Vladimir Stevanović
Vladimir Kuzminov
Wojciech Adamczyk
Wojciech Stanek
Yoshiharu Amano
Zornitza K-Yordanova
Zygmunt Kolenda

A regional model for the analysis of interconnected electricity markets in Central-Eastern Europe
Gerse Agnes, Börcsök Endre, ... 4211

The impact of weather conditions on the regional electricity supply adequacy in Central-Eastern Europe
Gerse Agnes, Börcsök Endre, Oláhné Groma Veronika, ... 4223

Role of acoustic fields on the fluidized bed carbonation for TCES in CSP applications
Raganati Federica, Chirone Riccardo, Ammendola Paola, ... 4237

Thermodynamic assessment on the integration of thermo-electric modules in a wood fireplace
Baldini Andrea, Cerofolini Luca, Fiaschi Daniele, Manfrida Giampaolo, Talluri Lorenzo, ... 4249

Exergoeconomic analysis for the optimal exploitation of heat in thermochemical storage units integrated with concentrated solar power
Guelpa Elisa, Capone Martina, Tesio Umberto, Verda Vittorio, ... 4261

High efficiency concentrated solar plant by increasing of power cycle temperature
Guelpa Elisa, Capone Martina, Tesio Umberto, Verda Vittorio, ... 4271

Evaluation of the extractive gold process: open-pit mining through exergy analysis
Orozco L Carlos A, Velasquez Héctor, Cano Natalia, Hasenstab Christian, ... 4283

First-principles study on the adsorption of hydrogen molecules on alkali-decorated germanene for energy storage
De Santiago Francisco, Sosa Akari, Miranda Álvaro, Trejo Alejandro, Pérez Luis, Cruz-Irisson Miguel, . 4297

Silicon carbide monolayer with alkali and alkaline earth metal adatoms for H2 storage: A computational study
De Santiago Francisco, Arellano Lucía, Miranda Álvaro, Salazar Fernando, Pérez Luis, Cruz-Irisson Miguel, ... 4311

Effect of radiant properties and heat transfer mechanisms on the thermal performance of a Calcium Looping carbonator reactor
Giménez-Gavarrell Pablo, Ortiz Carlos, Chacartegui Ricardo, Valverde José Manuel, ... 4323

Exergy analysis of the integration of a concentrated solar power plant with calcium looping for energy storage
Karasavvas Evgenios, Panopoulos Kyriakos, Papadopoulou Simira, Voutetakis Spyros, ... 4337

Exergo-economic and environmental analysis of a solar integrated thermo-electric storage
Fiaschi Daniele, Manfrida Giampaolo, Petela Karolina, Rossi Federico, Sinicropi Adalgisa, Talluri Lorenzo, ... 4349

A machine learning approach for predicting office energy consumption in a Mediterranean region
Hajj-Hassan Mohamad, Awada Mohamad, Khoury Hiam, Srour Issam, ... 4361

The role of the thermal processes of waste biomass in the circular economy perspective
Werle Sebastian, Sobek Szymon, Kaczor Zuzanna, ... 4373

Preliminary assessment of an integrated biomass-fired CHP plant with CO2 capture and enhanced geothermal system – Poland case study
Gładysz Paweł, Pająk Leszek, Sowiżdżał Anna, Miecznik Maciej, Hacaga Maciej, ... 4387

CO2 enhanced geothermal system for heat and electricity production – process configuration analysis for central Poland
Gładysz Paweł, Pająk Leszek, Sowiżdżał Anna, Miecznik Maciej, ... 4409

First-principles study on the adsorption of hydrogen molecules on alkali-decorated germanene for energy storage

Francisco de Santiago[a], Akari Narayama Sosa[b], Álvaro Miranda[c], Alejandro Trejo[d], Luis Antonio Pérez[e] and Miguel Cruz-Irisson[f]

[a] *Instituto Politécnico Nacional, ESIME-Culhuacán, Av. Santa Ana 1000, C.P. 04440, Ciudad de México, México*, fdesantiagov0900@alumno.ipn.mx ***CA***
[b] *Instituto Politécnico Nacional, ESIME-Culhuacán, Av. Santa Ana 1000, C.P. 04440, Ciudad de México, México, asosacamposeco@gmail.com*
[c] *Instituto Politécnico Nacional, ESIME-Culhuacán, Av. Santa Ana 1000, C.P. 04440, Ciudad de México, México, amirandad.ipn@gmail.com*
[d] *Instituto Politécnico Nacional, ESIME-Culhuacán, Av. Santa Ana 1000, C.P. 04440, Ciudad de México, México, alejandtb13@gmail.com*
[e] *Instituto de Física, Universidad Nacional Autónoma de México, Apartado Postal 20-364, 01000 Ciudad de México, México, lperez@fisica.unam.mx*
[f] *Instituto Politécnico Nacional, ESIME-Culhuacán, Av. Santa Ana 1000, C.P. 04440, Ciudad de México, México, irisson.ipn@gmail.com*

Abstract:

We have performed density functional theory-based calculations to study the geometrical structures and stability of pristine germanene, alkali atoms-adsorbed germanene and also the adsorption properties of H_2 molecules, ranging from one to seven molecules, on alkali atoms-decorated germanene. Using the information of adsorption energy of alkali atoms at different adsorption sites of a germanene supercell, it has been observed that the position at the center of one of the hexagons of the honeycomb structure is the preferred site for the adsorption of the alkali atoms. On comparing adsorption energy per H_2 molecule on pristine and alkali atoms-adsorbed germanene, we find that the presence of alkali atoms enhances the binding strength of H_2 molecules. The adsorption energy of the H_2 molecules to the alkali atoms is in the range of physisorption. The K-decorated germanene has the largest storage capacity, being able to bind up to seven H_2 molecules. These results may lead to materials with more hydrogen storage capacity for use in alternative energy sources.

Keywords:

2D materials, Density Functional Theory, Germanene, Hydrogen storage, Renewable energy storage

1. Introduction

Hydrogen is one of the most promising candidates for the replacement of current carbon-based energy sources because it is a source of clean energy that is abundant and has three times the energy per unit mass than that of hydrocarbons [1]. Although hydrogen is an ideal fuel there are many problems associated with its use, such as the cost of the production mechanism, which is at least

three times the cost of natural gas production [2,3], and storage efficiency [1,4]. The significance of storage efficiency can be seen when hydrogen fuel is used for mobile applications such as transportation where the high gravimetric density and the easy to store feature is needed. Among storage methods that exist today are compression, physisorption, metal hydrides via chemical reactions and liquefaction. Within these methods, physisorption is a good choice for applications due to its lightweight and easy-to-store features. Physisorption stores the hydrogen by means of low energy van der Waals attraction to a surface [5]. Research on several materials have shown that hydrogen can bind on surfaces either molecularly or through dissociative adsorption [6–10]. The challenge in physisorption-based storage is to find the most efficient and safe material for adsorption that would yield high gravimetric and volumetric density.

Most of the materials investigated involve carbon nanostructures due to their high surface area and reduced weight, particularly graphene [11–14]. Graphene, a two-dimensional honeycomb network of carbon atoms, is currently a material of much interest because of its unique electronic properties [15,16]. Unfortunately, graphene, with its high surface area, cannot hold that much hydrogen [5]. As a solution, some studies have used decorating atoms on graphene [17,18]. However, this decoration resulted in clustering that can significantly reduce the hydrogen storage capacity [19,20]. As an alternative, two-dimensional hexagonal lattices of Si and Ge, so called silicene and germanene [21,22], respectively, have been theoretically studied [23–25].

Pure germanium is a semiconductor with a smaller band gap than diamond and silicon and is regarded well in the transistor industry. Compared with graphene, germanene has a larger hexagonal lattice parameter. Germanene has been synthesized recently by several research groups [26–30]. A single-layer of fully hydrogenated germanene was also fabricated successfully [31]. Recently, atom adsorption on germanene is also studied [32,33]. Similar to silicene, atoms bind much stronger to germanene than graphene, which is mainly caused by the sp^2–sp^3 hybridization of Ge atom.

Little attention has been focused on hydrogen-molecule adsorption on germanene. Pang et al. [34] carried out a detailed investigation of the structural, energetic, and electronic properties of Li, Na and K atoms adsorbed on germanene for a wide range of coverages using first-principle methods, finding that these metals bind strongly to germanene. These results may be important to hydrogen storage on 2D materials because other theoretical investigations [35,36] have found that Li functionalization yields high H storage capacity without clustering. The use of alkali metals would be advantageous because these are the lightest elements on the periodic table, which theoretically would mean a high gravimetric capacity. A recent investigation by Rojas et al. [24] showed that K- and Ca-decorated germanene may adsorb up to 9 and 8 hydrogen molecules, respectively. Considering this, in this work we study the adsorption of several hydrogen molecules on Li-, Na- and K-decorated germanene.

2. Computational details

The total energy, electronic and geometrical structures of all systems studied in this work were obtained by means of Density Functional Theory (DFT) [37,38]. All calculations involved were performed using the SIESTA code [39]. The generalized gradient approximation (GGA) in the Perdew-Burke-Erzoff (PBE) [40] form was employed to describe the exchange and correlation energy. Optimized double-ζ polarized basis sets [41,42] and norm-conserving Troullier-Martins pseudopotentials [43] in their fully non-local form were used [44]. Since long-range interactions play a crucial role in the geometries and binding energies of the adsorbents, the effect of van der Waals interactions was taken into account by using the semiempirical method of Grimme with the inclusion of a long-range dispersion correction [45]. The real-space grid for numerical integrations was defined by an energy cutoff of 500 Ry. A supercell consisting of 4×4 germanene unit cells is employed for all the calculated structures. There is a vacuum layer of 30 Å along the z-direction to avoid interactions between adjacent periodic images. The 2D Brillouin zone was sampled with a Monkhorst-Pack grid [46] of 24 × 24 *k*-points. Geometric relaxations were performed by using a

conjugated gradient method as implemented in the SIESTA code, with no symmetry constraints. Atomic positions were allowed to relax until the force between any pair of atoms was lower than 0.01 eV/Å.

Fig. 1 shows the structure of germanene, we calculated the buckling value (perpendicular distance between the two Ge planes) as 0.74 Å. Upon the formation the of sp^3-bonded honeycomb lattice, the covalent bond length of Ge-Ge is 2.46 Å, with an angle between two adjacent bonds of 111.81°. The lattice parameter calculated of 4.12 Å is in good agreement with reported results [47,48]. The electron charge transfers between the germanene and the adsorbates were estimated by using Voronoi electronic population analysis [49]. All calculations of adsorption and binding energies are corrected for basis set superposition error with the counterpoise correction, as described by Boys et al [50].

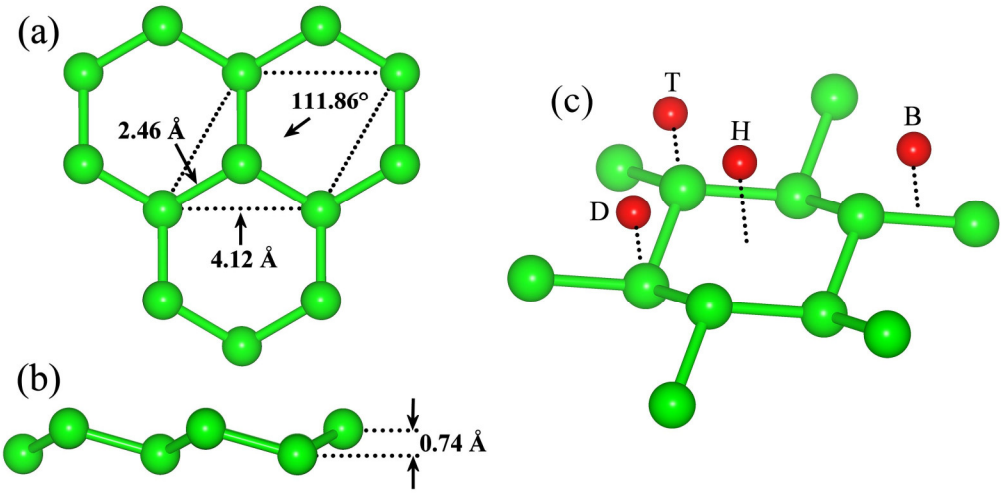

Figure 1. Atomic structure of germanene: (a) top view and (b) side view. (c) Preferred adsorption sites: hollow, top, down and bridge, on the germanene lattice. Green spheres represent germanium atoms. Red spheres represent any possible adsorbed atom.

3. Results and discussion

In order to address the possible use of germanene as hydrogen storage, we calculated the adsorption energies of H_2 molecules on pristine germanene and metal-adsorbed germanene. The adsorption energies (E_A) are calculated for three schemes: adsorption of H_2 molecules on pristine germanene, adsorption of alkali metal atoms on germanene, and adsorption of H_2 molecules on metal-adsorbed germanene.

3.1. Adsorption of a H_2 molecule on pristine germanene

In this section, we discuss the geometry and the stability of adsorption of H_2 on pristine germanene. We have considered a number of different initial geometric configurations to study the interaction between pristine germanene and a hydrogen molecule: the H_2 molecule was located over the monolayer with its bond axis in parallel and perpendicular orientations with respect to the monolayer (hereon referred to as horizontal and vertical orientations, respectively), and also we considered four different initial positions over the honeycomb lattice: the Hollow site (H), at the center of an hexagon; the Bridge site (B), over a Ge—Ge bond; and the Top and Down sites, over adjacent Ge atoms [see Fig. 1(c)].

The adsorption energy of a H_2 molecule on pristine germanene is calculated from the optimized geometry of a hydrogen-adsorbed germanene supercell using the next equation:

$$E_A = E_H + E_{Ger} - E_{H/Ger} + \Delta_{BSSE}, \quad (1)$$

where E_H is the total energy of a hydrogen molecule, E_{Ger} is the total energy of pristine germanene and $E_{H/Ger}$ is the total energy of the hydrogen-adsorbed germanene. Δ_{BSSE} refers to the basis set superposition error correction. All models are calculated using same-sized supercells of germanene.

Table 1 shows the adsorption energy and the H_2—germanene equilibrium distance for the four adsorption sites, and the two molecule orientations. The results show that the adsorption energy is the largest and the equilibrium distance is the shortest for a vertically oriented H_2 molecule at the H site of germanene, which means that this configuration is the most energetically stable of all modeled configurations. The calculated values of adsorption energy of H_2 on pristine germanene in the present work go from 0.18 to 0.2 eV. These energy values are bigger than previously reported values on graphene [51]. The small adsorption energy for single hydrogen adsorption is insufficient to be considered a chemical bond, and the molecule may be interacting with germanene through van der Waals forces. There are no chemically active sites on the germanene monolayer because all germanium atoms are bonded tetrahedrally. The repulsion between the electronic charge density of the molecule and the monolayer may be too strong to high the molecule to be more strongly adsorbed on the monolayer.

Table 1. Adsorption of a hydrogen molecule on pristine germanene. The adsorption sites are: top (T), down (D), hollow (H) and bridge (B). Adsorption energy of H_2 molecule (E_A), H_2-germanene distance (β), and Voronoi charge excess on the molecule (Q_V).

Orientation	Site	E_A (eV)	β (Å)	$Q_V(e)$
Vertical	T	0.180	3.310	0.032
	D	0.188	3.975	0.029
	H	0.206	3.807	0.046
	B	0.187	3.657	0.034
Horizontal	T	0.180	3.325	0.032
	D	0.187	3.960	0.029
	H	0.193	3.707	0.050
	B	0.188	3.337	0.034

For a further exploration of the interaction between pristine germanene and H_2 molecules, we calculate charge density difference (CDD) plots in our models using the next expression:

$$\Delta\rho(\mathbf{r}) = \rho_{H/Ger}(\mathbf{r}) - \rho_{Ge}(\mathbf{r}) - \rho_{H}(\mathbf{r}), \quad (2)$$

where $\rho_{H/Ger}$ is the electronic charge density of the system as whole, and ρ_H and ρ_{Ge} are the electronic charge densities of isolated H and Ge atoms, respectively, located at the same positions as they are in the system as a whole. The CDD plots are shown in Fig. 2, the cyan region represents charge accumulation [positive values of $\Delta\rho(\mathbf{r})$], while the purple region represents charge reduction [negative values of $\Delta\rho(\mathbf{r})$], both in reference to the charge density of isolated atoms.

The amount of charge transfer between the H_2 molecule and germanene is obtained by Voronoi electronic population analysis. Magnitudes of this transfer for all systems are presented in Table 1. For all cases the H_2 molecule can be considered an electron donor, however, the magnitude of the transfer is too small in comparison to a true chemical bond.

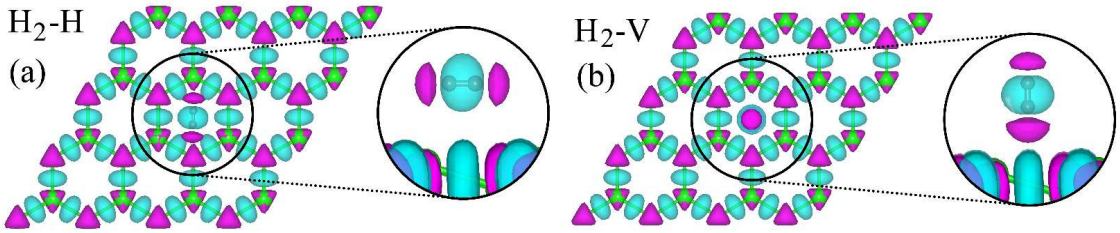

Figure 2. CDD plots for (a) horizontal and (b) vertical H_2-adsorption on pristine germanene, in both systems on the H site. Cyan regions represent the charge accumulation, while purple regions represent the charge depletion.

The CDD for the most favorable site, in both molecule orientations, is shown on Fig. 2. The H_2 molecule is not dissociated by its interaction with germanene, and there is no accumulation of charge that suggests a strong chemical bond with germanene atoms. The molecule favors the H site, at the center of the hexagon of the honeycomb lattice, where electronic density is less concentrated, and the repulsion between electronic clouds is weaker. Two zones of charge reduction can be seen close to the hydrogen atoms, and in the vertically oriented case, the zone closer to the germanene monolayer is slightly bigger, which may suggest that some of the electronic density from the hydrogen atom was transferred to the monolayer. This may account for the relatively larger adsorption energy in this case.

3.2. Adsorption of alkali atoms on germanene

In this section, we investigate the adsorption of alkali metal atoms on germanene. We explore the possible sites for the adsorption of the metallic atoms in the same way we did for the hydrogen molecule. The metal atom is placed in each of the possible places—top (T), down (D), hollow (H) and bridge (B)—and the supercell is geometrically optimized. The binding energy, as well as metal-germanene distance, charge transfer and CDD plots are calculated.

The resulting characteristic bonding geometry of the metal atoms in germanene is shown in Fig. 3. Upon full geometry optimization all Li, Na and K atoms favor the H site of the germanene. The adsorption of the metal atoms does not yield any significant distortion or stress on the germanene lattice. For all cases, the down site is the next favorable site.

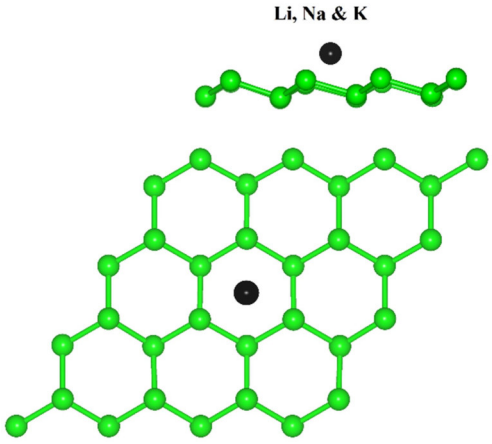

Figure 3. Side and top view for the most favorable adsorption geometry for metal atoms on germanene.

For all optimized metal-decorated germanene structures, we define the binding energy as:

$$E_{\mathrm{B}} = E_{\mathrm{alk}} + E_{\mathrm{ger}} - E_{\mathrm{alk/ger}} + \Delta_{\mathrm{BSSE}}, \tag{3}$$

where, E_{alk} is the total energy of an isolated alkali metal atom, E_{ger} is the total energy of the pristine germanene supercell and $E_{alk/ger}$ is the total energy of the metal-decorated germanene supercell. Δ_{BSSE} refers to the basis set superposition error correction. All models are calculated using same-sized supercells. The results of binding energy, as well as metal-germanene distance and charge transfer, are listed in Table 2.

The results show that once again the H site is the most energetically favorable. The calculated values of binding energy of metal atoms in the present work go from 2.08 to 2.64 eV. These energies are stronger than reported results for graphene (silicene), i.e., 1.1(2.4) eV for Li, 0.5(1.9) eV for Na and 0.8(2.1) eV for K, respectively [52]. The magnitude of the binding energy is well in the chemisorption range, and the magnitude of the Voronoi population suggests that the metals lose much larger electronic density to the monolayer than the case of H_2 adsorption. These results point towards the creation of a chemical bond between the metals and the monolayer.

Table 2. Calculated values of adatom adsorption on germanene. The adsorption sites are: top (T), down (D), hollow (H) and bridge (B). Binding energy of metal atom on germanene (E_B), adatom-germanene distance (β), and Voronoi charge excess on the metal atom (Q_V).

Metal atom	Site	E_B (eV)	β (Å)	$Q_V(e)$
Li	T	2.64	2.69	0.273
	D	2.31	2.71	0.360
	H	2.64	2.83	0.273
	B	2.64	2.83	0.273
Na	T	2.30	2.98	0.411
	D	2.08	2.99	0.466
	H	2.30	3.16	0.410
	B	2.08	3.04	0.466
K	T	2.37	3.35	0.514
	D	2.23	3.41	0.551
	H	2.37	3.57	0.512
	B	2.37	3.57	0.513

The calculated binding energies per atom of alkali atoms adsorbed on germanene, the corresponding binding energies of alkali atoms adsorbed on silicene [25] and cohesive energies of the respective alkali atoms [53] are shown in Fig. 4. For all metals, the binding energy for germanene is greater than for silicene. The binding energies for germanene are typically ~1 eV over the experimental cohesive energy of the bulk metals. This suggests that a metal adatom favors adsorption on the H site rather than binding with other metal atoms. Therefore, metal atoms do not tend to clusterize on the germanene monolayer. Clusterization would cause reduction of the metal's capacity to adsorb H_2 molecules.

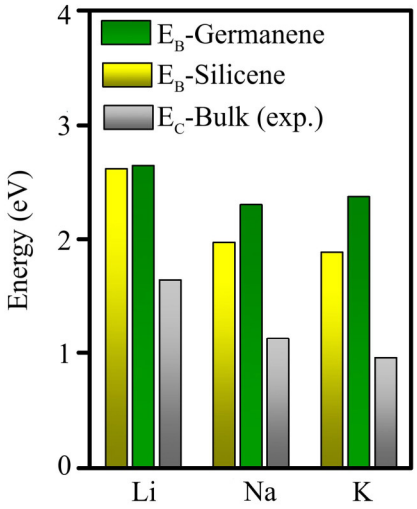

Figure 4. Calculated metal atom binding energies on germane (E_B-Germanene), binding energies on silicene (E_B-Silicene), and corresponding experimental cohesive energies of the bulk metals (E_C-Bulk experimental).

The CDD plots corresponding to the adsorption of metals are calculated using Eq. (2), with the electronic charge density of an isolated metal atom instead of the density of a hydrogen atom. The CDD plots are shown in Fig. 5.

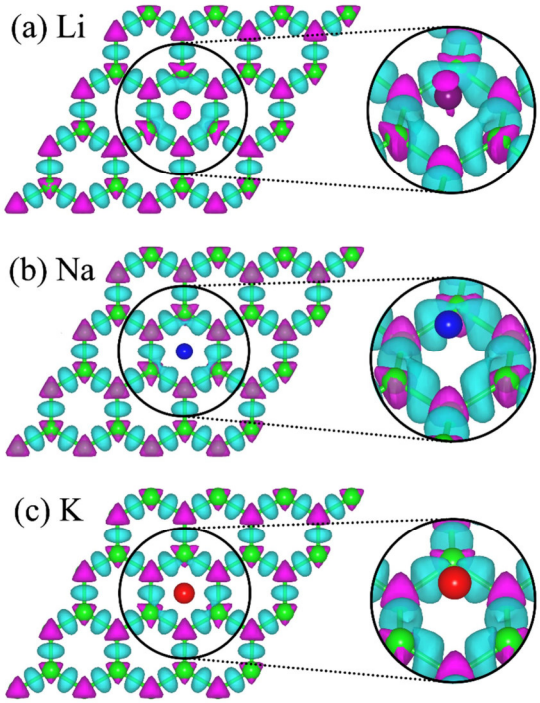

Figure 5. Charge density difference of (a) Li-, (b) Na- and (c) K-adsorption on pristine germanene, in the three systems on the hollow site.

There is an accumulation of electrons between two Ge first neighbors only in the hexagon where the metal is adsorbed. This accumulation may be electronic density that was transferred from the metal atom to the germanium lattice. As can be seen in the zoomed areas of Fig. 5, the accumulation on the Ge bonds diminishes from Li to K. There is a small surface of charge reduction around the Li. This suggests that Li transfers more electronic density to the monolayer, followed by Na and K. This tendency matches the calculated Voronoi charge on the metal (less charge on Li, more charge on K), the metal-germanene distance (increasing from Li to K) and the ability of the alkali metals to

lose electrons, as given by their ionization energies and electropositivity. This electronic density redistribution, more noticeable than on the case of H_2 adsorption, points towards a chemical bond between the germanene lattice and the metal adatom.

3.3. Adsorption of H_2 molecules on alkali metal decorated germanene

On the basis of the above investigation of alkali metal decorated germanene systems, in the following, we turn to the discussion on the adsorption of H_2 molecules on these systems. The adsorption of several hydrogen molecules is calculated using the next equation:

$$E_A = NE_H + E_{alk/ger} - E_{H/alk/ger} + \Delta_{BSSE}, \quad (3)$$

where E_H, $E_{alk/ger}$ and $E_{H/alk/ger}$ are the total energies of an isolated H_2 molecule, metal-decorated germanene and metal-decorated germanene after adsorbing an N number of molecules. Δ_{BSSE} refers to the basis set superposition error correction. Positive adsorption energies signify that H_2 molecules tend to be adsorbed by the metal-decorated germanene

In these models, an increasing number of H_2 molecules were placed around the metal atom, at a distance of ~1 Å and on a symmetric configuration, on the geometrically optimized metal-decorated germanene. The models with the H_2 molecules were then geometrically optimized again. Fig. 6 shows the optimized structures of metal-decorated germanene with the maximum number of H_2 molecules it can adsorb: Li can adsorb 3, while Na and K can adsorb up to 7 H_2 molecules. The results of adsorption energy per H molecule and its average distance from metal-decorated germanene are listed in Table 3.

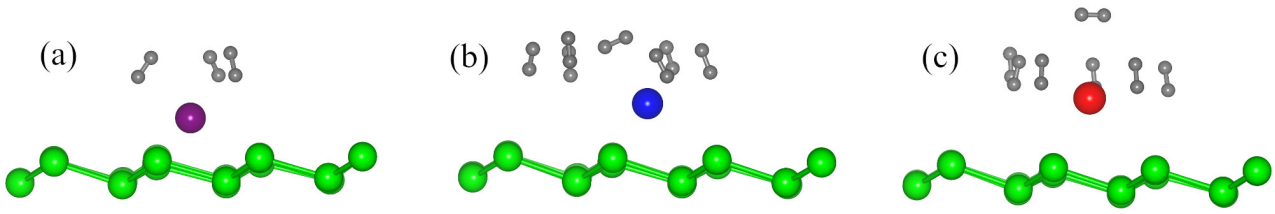

Figure 6. Optimized structures of Li-, Na-, and K-decorated germanene with the maximum number of H_2 molecules they can adsorbed.

Table 3 shows the adsorption energy per H_2 molecule. If we compare the adsorption energy with and without metal atoms, it can be seen that only Li improves the adsorption strength. The magnitude of the adsorption energy of H_2 on pristine germanene has a value between the adsorption with Li and with Na. All values are still in the range of physisorption, which is favorable for hydrogen storage applications, as it means that the energy required for desorbing the molecules is not as much as the needed to dissociate H—metal chemical bonds. Note that the H—H bonds never break, their bond length is consistently 0.79 eV.

Table 3. Adsorption energy per H_2 molecule (E_A) on metal-decorated germanene, molecules-metal atom average distance (α), average Voronoi H_2 charge excess (Q_V), and average H—H bond distance (β).

Atom	Number of H_2 molecules	E_A (eV)	α (Å)	Q_V (e)	β (Å)
Li	1	0.28	1.965	0.170	0.79
	2	0.23	2.017	0.105	0.79
	3	0.21	2.030	0.087	0.79
Na	1	0.18	2.335	0.176	0.79
	2	0.19	2.355	0.121	0.79
	3	0.19	2.358	0.104	0.79
	4	0.18	2.388	0.081	0.79
	5	0.16	2.511	0.065	0.79
	6	0.15	2.524	0.055	0.79
	7	0.14	2.940	0.051	0.79
K	1	0.13	2.700	0.195	0.79
	2	0.18	2.682	0.135	0.79
	3	0.18	2.688	0.116	0.79
	4	0.18	2.693	0.105	0.79
	5	0.18	2.690	0.088	0.79
	6	0.18	2.705	0.074	0.79
	7	0.16	3.032	0.066	0.79

In Fig. 7 the adsorption energies obtained in the present work are compared with theoretical data obtained in other works. The case with lithium, is compared with silicene (red) [25], SiC monolayer (black) [54], and Li-coated B_{80} buckyballs (magenta) [55]. Except for the case of one molecule, the values are very similar. The case with sodium is compared with silicene (red) [25], Na-coated B_{80} buckyballs (magenta) [55], and graphene (blue) [51]. The graphene has values considerably different to the other materials, but silicene and germanene are very similar, and adsorb the same number of molecules. Na-coated buckyballs have also similar values but can adsorb only one molecule. The case with potassium is compared with silicene (red) [25], K-coated B_{80} buckyballs (magenta) [55], and germanene (dark green) [24]. K-coated B_{80} buckyballs have very low values and can only adsorb one molecule. Silicene is again very close to our results. Values for K-decorated germanene are available in the literature, which are in very good agreement with ours, except for a constant difference in magnitude which can be attributed to the exchange-correlation functional used.

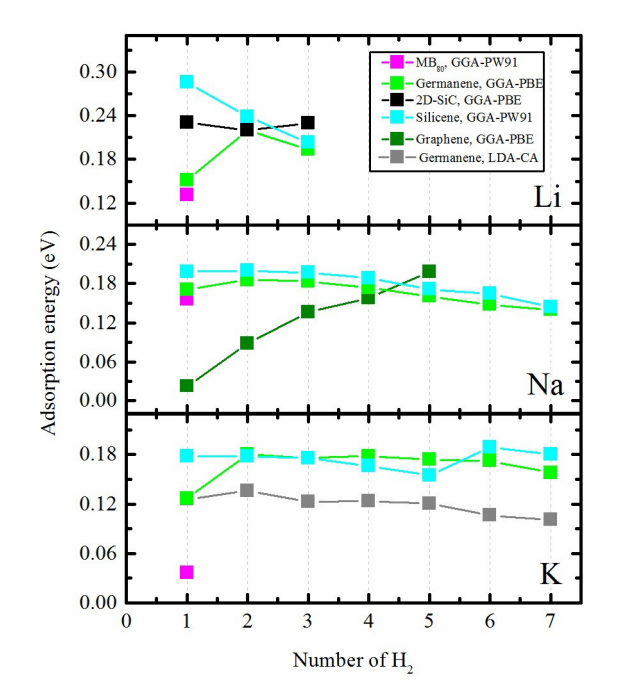

Figure 7. Adsorption energy per H_2 molecule for Li-, Na-, and K-adsorbed on germanene (light green), compared with other nanomaterials: silicene (GGA-PW91) (cyan), 2D-SiC (GGA-PBE) (black) sheet, MB_{60} (GGA-PW91) (magenta), graphene (GGA-PBE) (green), and germanene (LDA-CA) (gray).

Conclusions

In summary, we have investigated metal-decorated germanene as a hydrogen storage nanostructure using first-principles calculations. The results show that pristine germanene does not have high storage capacity to H_2, as it can adsorb only one hydrogen molecule per site. Adsorption energies of hydrogen on pristine and metal-decorated germanene are comparable, but Li-decorated germanene can store up to 3 molecules, while the Na and K cases can store up to 7 molecules.

It was also found that the binding energy of the metal adatoms to the hollow site on the germanene monolayer is too strong to allow the clustering of the metal adatoms, as has been predicted on graphene or other carbon-based nanostructures as a hydrogen storage material. The values of adsorption energy and capacity are very close to the reported results for silicene monolayers. The results of binding of alkali atoms on some sites on germanene may be significant in the exploration of potential applications of germanene not only in hydrogen-related technologies, but also in electrodes for alkali-ion batteries.

Acknowledgments

This work was partially supported by multidisciplinary projects IPN-SIP 2018-1937, individual project IPN-SIP 2019-5830, and UNAM-PAPIIT IN107717. Computations were performed at the supercomputer Miztli of DGTIC-UNAM (Project LANCAD-UNAM-DGTIC-180), at supercomputer Abacus-I of CINVESTAV-EDOMEX, and at the supercomputer Xiuhcóatl of CINVESTAV (Project LANCAD). F.S. and A.N.S. would like to thank BEIFI-IPN, CONACYT and COFAA-IPN for their financial support.

References

[1] Schlapbach L, Züttel A. Hydrogen-storage materials for mobile applications. Nature. 2001 Nov 15;414:353.

[2] Gaudernack B, Lynum S. Hydrogen from natural gas without release of CO2 to the atmosphere. Int J Hydrogen Energy. 1998;23(12):1087–93.

[3] Garland NL, Papageorgopoulos DC, Stanford JM. Hydrogen and Fuel Cell Technology: Progress, Challenges, and Future Directions. Energy Procedia . 2012;28:2–11.

[4] Zhou L. Progress and problems in hydrogen storage methods. Renew Sustain Energy Rev. 2005;9(4):395–408.

[5] Ding F, Yakobson BI. Challenges in hydrogen adsorptions: from physisorption to chemisorption. Front Phys. 2011;6(2):142–50.

[6] B. Arboleda N, Nobuhara K, Kasai H, A. Diño W, Nakanishi H. First Principles Studies for the Interaction of Hydrogen with a Li(100) Surface. J Phys Soc Japan. 2005;74(1):478–82.

[7] Kobayashi H, Yoshida S, Kato H, Fukui K, Tarama K. Theoretical studies of hydrogen molecule adsorption on flat and stepped platinum surfaces. Surf Sci . 1979;79(1):189–204.

[8] Granja A, Alonso JA, Cabria I, López MJ. Competition between molecular and dissociative adsorption of hydrogen on palladium clusters deposited on defective graphene. RSC Adv . 2015;5(59):47945–53.

[9] Dürr M, Höfer U. Dissociative adsorption of molecular hydrogen on silicon surfaces. Surf Sci Rep. 2006;61(12):465–526.

[10] Henry DJ, Yarovsky I. Dissociative Adsorption of Hydrogen Molecule on Aluminum Clusters: Effect of Charge and Doping. J Phys Chem A . 2009;113(11):2565–71.

[11] Novoselov KS, Geim AK, Morozov S V, Jiang D, Zhang Y, Dubonos S V, et al. Electric Field Effect in Atomically Thin Carbon Films. Science. 2004;306(5696):666 LP-669.

[12] Gallouze M, Kellou A, Drir M. Electronic and magnetic properties of adsorbed H2 on graphene with atomic defects: Ab initio study. Phys E Low-dimensional Syst Nanostructures. 2013;52:127–35.

[13] Lee CH, Chen SC, Su WS, Chen RB, Lin MF. Tuning the electronic properties of monolayer graphene by the periodic aligned graphene nanoribbons. Synth Met. 2011;161(5):489–95.

[14] Enriquez JIG, Villagracia ARC. Hydrogen adsorption on pristine, defected, and 3d-block transition metal-doped penta-graphene. Int J Hydrogen Energy. 2016;41(28):12157–66.

[15] Geim AK, Novoselov KS. The rise of graphene. Nat Mater. 2007;6:183.

[16] Castro Neto AH, Guinea F, Peres NMR, Novoselov KS, Geim AK. The electronic properties of graphene. Rev Mod Phys. 2009;81(1):109–62.

[17] Cho JH, Yang SJ, Lee K, Park CR. Si-doping effect on the enhanced hydrogen storage of single walled carbon nanotubes and graphene. Int J Hydrogen Energy. 2011;36(19):12286–95.

[18] Denis PA, Huelmo CP, Iribarne F. Theoretical characterization of sulfur and nitrogen dual-doped graphene. Comput Theor Chem. 2014;1049:13–9.

[19] Sun Q, Wang Q, Jena P, Kawazoe Y. Clustering of Ti on a C60 Surface and Its Effect on Hydrogen Storage. J Am Chem Soc. 2005;127(42):14582–3.

[20] Faye O, Eduok U, Szpunar J, Szpunar B, Samoura A, Beye A. Hydrogen storage on bare Cu atom and Cu-functionalized boron-doped graphene: A first principles study. Int J Hydrogen Energy. 2017;42(7):4233–43.

[21] Cahangirov S, Topsakal M, Aktürk E, Şahin H, Ciraci S. Two- and One-Dimensional Honeycomb Structures of Silicon and Germanium. Phys Rev Lett. 2009;102(23):236804.

[22] Houssa M, Scalise E, Sankaran K, Pourtois G, Afanas'ev V V, Stesmans A. Electronic properties of hydrogenated silicene and germanene. Appl Phys Lett 2011 May 30;98(22):223107.

[23] Li F, Zhang C, Luan H, Wang P. First-principles study of hydrogen storage on Li-decorated silicene. J Nanoparticle Res. 2013;15(10):1972.

[24] Rojas KIM, Villagracia ARC, Moreno JL, David M, Arboleda NB. Ca and K decorated germanene as hydrogen storage: An ab initio study. Int J Hydrogen Energy.

2018;43(9):4393–400.

[25] Wang Y, Zheng R, Gao H, Zhang J, Xu B, Sun Q, et al. Metal adatoms-decorated silicene as hydrogen storage media. Int J Hydrogen Energy. 2014;39(26):14027–32.

[26] Lay MED and LX and SC and AR and G Le. Germanene: a novel two-dimensional germanium allotrope akin to graphene and silicene. New J Phys. 2014;16(9):95002.

[27] Li L, Lu SZ, Pan J, Qin Z, Wang YQ, Wang Y, et al. Buckled germanene formation on Pt(111). Adv Mater. 2014;26(28):4820–4.

[28] Bampoulis P, Zhang L, Safaei A, Van Gastel R, Poelsema B, Zandvliet HJW. Germanene termination of Ge2Pt crystals on Ge(110). J Phys Condens Matter. 2014;26(44).

[29] D'Acapito F, Torrengo S, Xenogiannopoulou E, Tsipas P, Marquez Velasco J, Tsoutsou D, et al. Evidence for Germanene growth on epitaxial hexagonal (h)-AlN on Ag(1 1 1). J Phys Condens Matter. 2016;28(4).

[30] Derivaz M, Dentel D, Stephan R, Hanf M-C, Mehdaoui A, Sonnet P, et al. Continuous Germanene Layer on Al(111). Nano Lett. 2015;15(4):2510–6.

[31] Bianco E, Butler S, Jiang S, Restrepo OD, Windl W, Goldberger JE. Stability and Exfoliation of Germanane: A Germanium Graphane Analogue. ACS Nano. 2013;7(5):4414–21.

[32] van den Broek B, Houssa M, Scalise E, Pourtois G, Afanas'ev V V, Stesmans A. First-principles electronic functionalization of silicene and germanene by adatom chemisorption. Appl Surf Sci. 2014;291:104–8.

[33] Ye M, Quhe R, Zheng J, Ni Z, Wang Y, Yuan Y, et al. Tunable band gap in germanene by surface adsorption. Phys E Low-dimensional Syst Nanostructures. 2014;59:60–5.

[34] Pang Q, Zhang C, Li L, Fu Z, Wei X, Song Y. Adsorption of alkali metal atoms on germanene: A first-principles study. Appl Surf Sci. 2014;314:15–20.

[35] Zhang X, Tang C, Jiang Q. Electric field induced enhancement of hydrogen storage capacity for Li atom decorated graphene with Stone-Wales defects. Int J Hydrogen Energy. 2016;41(25):10776–85.

[36] Hussain T, Pathak B, Adit Maark T, Moyses Araujo C, Scheicher RH, Ahuja R. Ab initio study of lithium-doped graphane for hydrogen storage. EPL. 2011;96(2):27013.

[37] Hohenberg P, Kohn W. Inhomogeneous Electron Gas. Phys Rev . 1964;136(3B):B864–71.

[38] Kohn W, Sham LJ. Self-Consistent Equations Including Exchange and Correlation Effects. Phys Rev. 1965;140(4A):A1133–8.

[39] Sánchez-Portal JMS and EA and JDG and AG and JJ and PO and D. The SIESTA method for ab initio order- N materials simulation. J Phys Condens Matter. 2002;14(11):2745.

[40] Perdew JP, Burke K, Ernzerhof M. Generalized Gradient Approximation Made Simple. Phys Rev Lett. 1996 (18):3865–8.

[41] Artacho E, Sánchez-Portal D, Ordejón P, García A, Soler JM. Linear-Scaling ab-initio Calculations for Large and Complex Systems. Phys status solidi. 1999;215(1):809–17.

[42] Junquera J, Paz Ó, Sánchez-Portal D, Artacho E. Numerical atomic orbitals for linear-scaling calculations. Phys Rev B. 2001;64(23):235111.

[43] Troullier N, Martins JL. Efficient pseudopotentials for plane-wave calculations. Phys Rev B. 1991 ;43(3):1993–2006.

[44] Kleinman L, Bylander DM. Efficacious Form for Model Pseudopotentials. Phys Rev Lett. 1982;48(20):1425–8.

[45] Grimme S. Semiempirical GGA-type density functional constructed with a long-range dispersion correction. J Comput Chem. 2006;27(15):1787–99.

[46] Monkhorst HJ, Pack JD. Special points for Brillouin-zone integrations. Phys Rev B [Internet]. 1976;13(12):5188–92.

[47] Gupta SK, Singh D, Rajput K, Sonvane Y. Germanene: a new electronic gas sensing material. RSC Adv. 2016;6(104):102264–71.

[48] Hussain T, Kaewmaraya T, Chakraborty S, Vovusha H, Amornkitbamrung V, Ahuja R. Defected and Functionalized Germanene-based Nanosensors under Sulfur Comprising Gas Exposure. ACS Sensors. 2018;3(4):867–74.

[49] Fonseca Guerra C, Handgraaf J-W, Baerends EJ, Bickelhaupt FM. Voronoi deformation density (VDD) charges: Assessment of the Mulliken, Bader, Hirshfeld, Weinhold, and VDD methods for charge analysis. J Comput Chem. 2004;25(2):189–210.

[50] Boys SF, Bernardi F. The calculation of small molecular interactions by the differences of separate total energies. Some procedures with reduced errors. Mol Phys. 1970;19(4):553–66.

[51] Pantha N, Belbase K, Adhikari NP. First-principles study of the interaction of hydrogen molecular on Na-adsorbed graphene. Appl Nanosci . 2015;5(4):393–402.

[52] Sahin H, Peeters FM. Adsorption of alkali, alkaline-earth, and 3d transition metal atoms on silicene. Phys Rev B. 2013;87(8):85423.

[53] Kittel C. Introduction to Solid State Physics. Wiley; 2004.

[54] Song N, Wang Y, Zheng Y, Zhang J, Xu B, Sun Q, et al. New template for Li and Ca decoration and hydrogen adsorption on graphene-like SiC: A first-principles study. Comput Mater Sci. 2015;99:150–5.

[55] Wu G, Wang J, Zhang X, Zhu L. Hydrogen Storage on Metal-Coated B80 Buckyballs with Density Functional Theory. J Phys Chem C. 2009;113(17):7052–7.

Silicon carbide monolayer with alkali and alkaline earth metal adatoms for H_2 storage: a computational study

Francisco de Santiago[a], Lucía Arellano[b], Álvaro Miranda[c], Fernando Salazar[d], Luis A. Pérez[e] and Miguel Cruz-Irisson[f]

[a] *Instituto Politécnico Nacional, ESIME-Culhuacán, Av. Santa Ana 1000, C.P. 04440, Ciudad de México, México, fdesantiagov0900@alumno.ipn.mx* ***CA***
[b] *Instituto Politécnico Nacional, ESIME-Culhuacán, Av. Santa Ana 1000, C.P. 04440, Ciudad de México, México, lucia.arellano.gin2017@gmail.com*
[c] *Instituto Politécnico Nacional, ESIME-Culhuacán, Av. Santa Ana 1000, C.P. 04440, Ciudad de México, México, amirandad.ipn@gmail.com*
[d] *Instituto Politécnico Nacional, ESIME-Culhuacán, Av. Santa Ana 1000, C.P. 04440, Ciudad de México, México, fsalazarp@ipn.mx*
[e] *Instituto de Física, Universidad Nacional Autónoma de México, Apartado Postal 20-364, 01000 Ciudad de México, México, lperez@fisica.unam.mx*
[f] *Instituto Politécnico Nacional, ESIME-Culhuacán, Av. Santa Ana 1000, C.P. 04440, Ciudad de México, México, irisson.ipn@gmail.com*

Abstract:

Given their great surface-to-volume ratio, bidimensional monolayers are ideal for hydrogen storage in fuel cell systems. It has been demonstrated that the silicon carbide (SiC) monolayer has a sp^2 hybridization which makes it an alternative to graphene. In this work, the hydrogen adsorption properties of a silicon carbide monolayer decorated with alkali and alkaline earth metal atoms are analysed by means of first-principles calculations. The results suggest that the adatoms cause little distortion to the monolayer, and they tend to be adsorbed on sites above Si atoms. The adatoms act as adsorption sites for H_2 molecules: up to seven molecules can be adsorbed by K, Mg and Ca. The adsorption energies suggest that H_2 molecules are physisorbed over the decorated SiC monolayer, which means that no chemical bonds are created between H_2 and the adatoms. This is beneficial because the breaking of chemical bonds, which would be needed to make use of the stored H_2, is energetically expensive. These results add to a continuing effort to develop efficient means of reversible hydrogen storage.

Keywords:

2D materials, Alkali metals, Density Functional Theory, Hydrogen storage, Silicon carbide.

1. Introduction

Silicon carbide has attracted much interest due to its useful properties: resistance to corrosion, large band gap (3.2 eV), high mechanical strength, low density, high hardness, high thermal conductivity

and low thermal expansion coefficient (1–3). Several theoretical studies have investigated the atomic structure and electronic properties of nanostructured SiC as a promising material for the next generation of nanoelectronics and energy applications (4); for example, nanoporous SiC (5–7), nanotubes for energy storage (8) or nanowires for optoelectronics (9–11). Nanostructured SiC has also been synthesized as nanohole arrays (12), nanowires for piezoelectronics (13) or thin films for thermal sensors (14).

Among the different nanoscale structures that can be investigated, 2D materials have been given extensive attention in recent years since the rise of graphene. A number of applications have been found for this type of materials, including p−n junctions and transistors (15,16), gas sensors (17,18), spintronics (19), components for Li−ion and Na−ion batteries (20), and so on. Similar to graphene in its honeycomb structure, sp^2 bonding and flatness (21), a SiC monolayer could exhibit a large band gap and benefit from the advantageous properties of SiC, while having the potential applications in which 2D materials excel. At the time of writing, ultrathin SiC nanoflakes and nanosheets have been successfully synthesized (15,22,23).

The study of the adsorption mechanisms of H_2 on solid-state materials is essential for the widespread adoption of hydrogen as an energy carrier, which has been demonstrated to be cleaner and more available than fossil fuels (24,25). Storage by solid state materials provides advantages over compressed gas or liquefaction, which would require great quantities of energy to produce the appropriate temperatures and pressures (25). The nanostructuring of materials greatly extends their usable surface area per volume unit, and this improves their adsorption properties (26,27). This application relies on the ability of the host material to adsorb H_2 molecules, although a strong bonding is not favourable since it would make difficult the cleaning and reuse of the host material.

H_2 adsorption can be achieved using functionalizing atoms deposited on a substrate (28–30). Transition metals have been used in several materials, however, clustering of these atoms tends to happen, which hinders the adsorption of H_2 molecules (31–33).

Given the potential advantages of a SiC monolayer, we propose it as a possible substrate for the storage and detection of molecular hydrogen. To avoid the use of transition metals, we explore the potential use of alkali and alkaline-earth metal atoms decorating the monolayer as H_2 adsorption sites. Besides preventing the formation of metal clusters, the use of alkali and alkaline-earth metals would reduce the weight of the storage system and increase its gravimetric capacity. A recent work (34) reported the adsorption of alkali and alkaline metals on a SiC monolayer by means of DFT. The work described the possibility of hydrogen and oxygen evolution reactions using free energy calculations. Another paper (35) explored the cases of Li- and Ca-decorated SiC monolayers. However, a systematic study of the capacity of metal-decorated SiC monolayers to adsorb a number of H_2 molecules, as has been carried out for graphene (36) or silicene (29), is still absent from the literature.

In this paper, the properties of the pristine SiC monolayer are first obtained. Subsequently, an alkali or alkaline-earth metal atom is placed on different possible adsorption sites on a SiC monolayer supercell, and the most favourable site is chosen. On this site, from 1 to 7 hydrogen molecules are placed, to evaluate the adsorption on the monolayer and how it is affected by the number of H_2 molecules in the proximity. For comparison, the possible case of a H_2 molecule adsorbed on the pristine SiC monolayer is also calculated.

2. Computational details

Density Functional Theory (37,38) was used to calculate the total energy of all systems, by means of the SIESTA method (39). Exchange and correlation potentials were calculated through the PBE functional (40), within the GGA approximation. A double-ζ polarized basis set was used (41,42), as well as Troullier-Martin's norm-conserving pseudopotentials (43) in a fully non-local form (44). The real space grid for numerical integrations was defined by a cut-off energy of 460 Ry. A reciprocal-space grid of 24×24×1 was generated by the Monkhorst-Pack technique (45). Atomic structures were optimized using a conjugate gradient algorithm, as implemented in the SIESTA

code, until the force between any pair of atoms was less than 0.001 eV/Å. To calculate the resulting electronic charge correspondent to each atom, and evaluate their gain or loss of electrons, Voronoi electronic population analysis was employed (46).

The decorated monolayers with a variating number of H_2 molecules were all modelled in a 5×5 SiC-monolayer supercell. Periodic boundary conditions are used, and to avoid unwanted interactions, a distance of 10 Å separates the monolayer from its artificial image along its z direction.

3. Results and discussion

As the first step, the pristine SiC monolayer is geometrically optimized. Its structural characteristics are shown in Fig. 1. The Si–C bond length is 1.8 Å, while the lattice parameter is 3.11 Å. As with graphene, sp^2 hybridization allows the structure to be flat, unlike silicene and other 2D materials. This structure is a semiconductor with a band gap of 2.04 eV, the corresponding density of states is shown in Fig. 2. These values are close to those reported in the literature with more expensive calculation techniques (34).

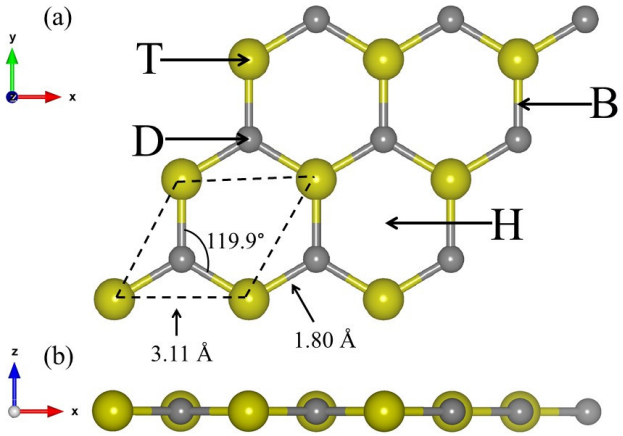

Figure 1. (a) Top view of a fragment of the SiC monolayer. T, D, H and B are adsorption sites. The primitive cell is marked by dashed lines. (b) Side view of the fragment.

There are various adsorption sites for the metal atoms (see Fig. 1). On the optimized pristine SiC monolayer, a metal atom is placed in each of the sites and the system is geometrically optimized, to evaluate the most energetically favourable site for metal adsorption. Table 1 summarizes the results for each metal. The adsorption energy is calculated according to the next formula:

$$E_a = E_M + E_{SiC} - E_{SiC+M}, \quad (1)$$

where E_M is the total energy of an isolated metal atom, E_{SiC} is the total energy of the pristine SiC monolayer supercell, and E_{SiC+M} is the total energy of the optimized system of the monolayer supercell with the decorating metal atom. The adsorption energies fall in the range of chemisorption (47), that is, all metal atoms are bonded to the SiC monolayer, except for the Mg atom, which has an adsorption energy under 0.5 eV, and a very low charge transfer to the monolayer. The most favourable site for all metals was the T site, over a Si atom, which concurs with the site found by Baierle et al. (34) and Song et al. (35). The reason for this preference may arise from the known fact that, in the Si—C bonds, C tends to strongly attract the electronic cloud from the Si, given its larger electronegativity. The Si is thus ionized and creates a positively charged region which electrostatically attracts the electronic cloud from the metals. Moreover, the Si atoms on the SiC monolayer have an open p-shell, which can readily accommodate one electron to complete the octet.

Table 1. Results for adsorption of metal atoms on each site of the monolayer: adsorption energies (E_a), metal-monolayer distance (h) and charge transfer from the metal atom (Q_V).

Metal	Site	E_a (eV)	h (Å)	Q_V ($\|e\|$)
Li	B	1.23	2.74	0.41
	T	1.23	2.74	0.41
	D	0.86	2.67	0.38
	H	1.23	2.54	0.41
Na	B	0.88	2.75	0.48
	T	0.88	2.76	0.48
	D	0.63	2.95	0.36
	H	0.72	2.78	0.39
K	B	1.01	3.15	0.51
	T	1.01	3.15	0.51
	D	0.84	3.03	0.51
	H	1.01	3.15	0.51
Be	B	0.25	2.84	0.10
	T	0.68	2.18	0.30
	D	0.15	3.58	0.03
	H	0.29	3.05	0.04
Mg	B	0.31	3.19	0.10
	T	0.31	3.18	0.10
	D	0.30	3.68	0.04
	H	0.31	3.29	0.05
Ca	B	0.60	3.01	0.47
	T	0.60	3.01	0.47
	D	0.36	3.81	0.15
	H	0.36	3.56	0.08

The adsorption of the metal causes a small displacement out of the plane of the Si atom below, but otherwise the monolayer has no important distortion. The calculation of the partial density of states (see Fig. 2) for each of the metal-decorated shows that in all cases there are occupied states with contribution from the metal and Si, which suggests a hybridization of atomic orbitals and the possible formation of a chemical bond. This is favourable because this atom will serve as adsorption centre for H_2 molecules. All the structures are semiconductors.

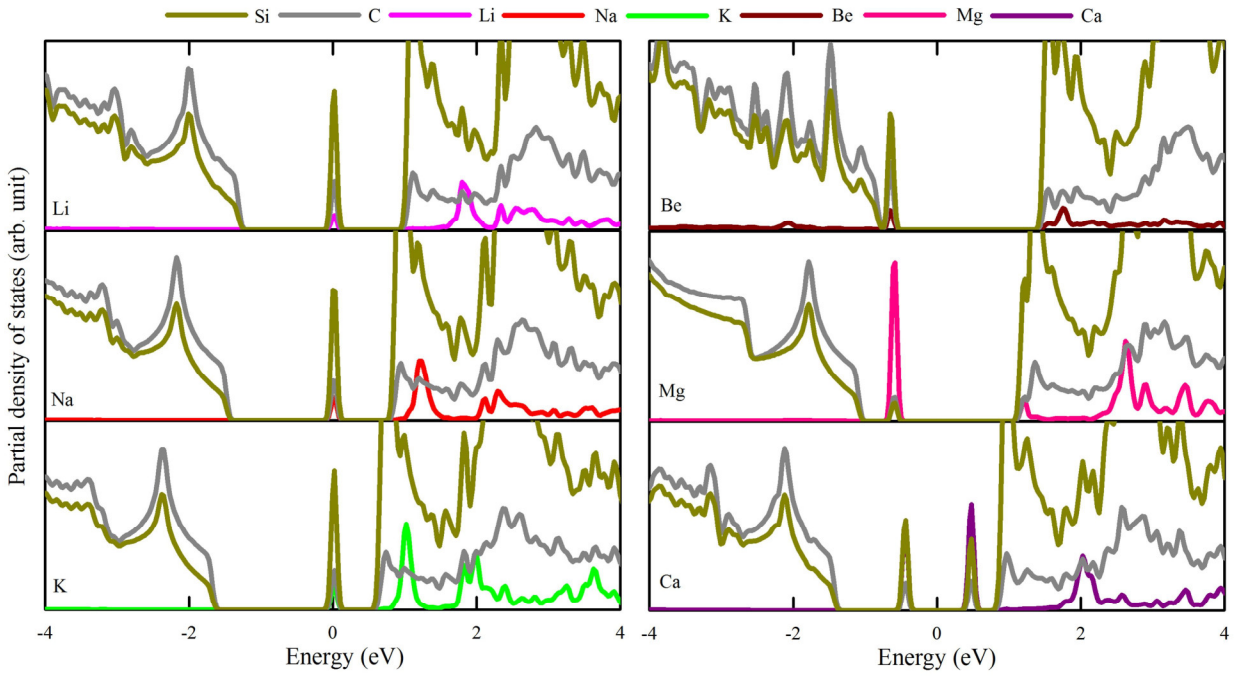

Figure 2. Partial densities of states of the alkali and alkaline-earth metals-decorated monolayer. The Fermi level is set to zero.

The possibility of the metal atoms clustering, which would be detrimental to the hydrogen storage capacity of the monolayer, is evaluated by comparing the adsorption energy of each metal to the SiC with the cohesive energy of each metal in its stable bulk form (48) (see Fig. 3). If the bulk cohesive energy is larger, the metal atoms prefer to bond together than disperse evenly on the monolayer, which may cause the creation of metal clusters. In the opposite case, the single metal atoms tend to be dispersed through the monolayer. Our results are compared with those obtained theoretically for silicene and graphene (29), showing that the only case in which the cohesive bulk energy is smaller is that of K. The monolayer-metal binding energies lie between graphene and silicene, but in all cases, values for silicene are more than 100% larger.

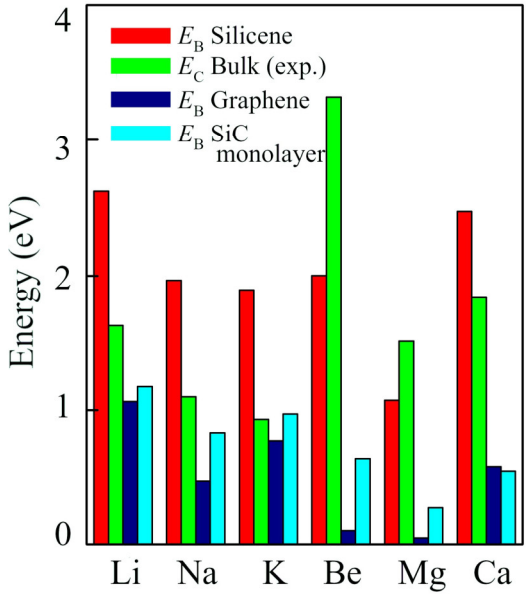

Figure 3. Comparison of calculated metal binding energies on SiC monolayer (BE SiC), with the cases of graphene (BE Graphene), silicene (BE Silicene), and the experimental cohesive energies (CE) of the bulk alkali and alkaline-earth metals.

Now we turn to the analysis of the interaction between H_2 and the pristine SiC monolayer. We carried out the tests for the most stable adsorption site for H_2, and for the most favourable position: a case where the molecular axis is perpendicular to the monolayer plane, and a case where it is parallel. This is evaluated using the next equation for the adsorption energy:

$$E_a = E_H + E_{SiC} - E_{SiC+H}, \quad (2)$$

where E_H is the total energy of a hydrogen molecule, E_{SiC} is the total energy of the pristine SiC monolayer supercell, and E_{SiC+H} is the total energy of the optimized system of the monolayer supercell with a hydrogen molecule. The results are shown on Table 2. The preferred site is the H, and the preferred orientation is perpendicular. The partial densities of states of the pristine and the H_2-adsorbed monolayers is shown in Fig. 4. The states from H are concentrated around 6 and -6 eV and cause only a small change in the curves of Si and C, which means that a chemical bond between the molecule and the monolayer is unlikely. Although the adsorption energy is in the range of physisorption, only one H_2 molecule can be adsorbed in the H site on the pristine monolayer.

Table 2. Results for adsorption of one H_2 molecule on the pristine monolayer: adsorption energies (E_a), molecule-monolayer distance (h) and charge transfer from the molecule (Q_V).

H_2 orientation	Site	E_a (eV)	h (Å)	Q_V ($\|e\|$)
Perpendicular	B	0.11	2.78	0.05
	T	0.10	2.83	0.05
	D	0.11	2.76	0.05
	H	0.13	2.50	0.05
Parallel	B	0.11	2.79	0.04
	T	0.10	2.94	0.07
	D	0.12	2.61	0.06
	H	0.12	2.60	0.05

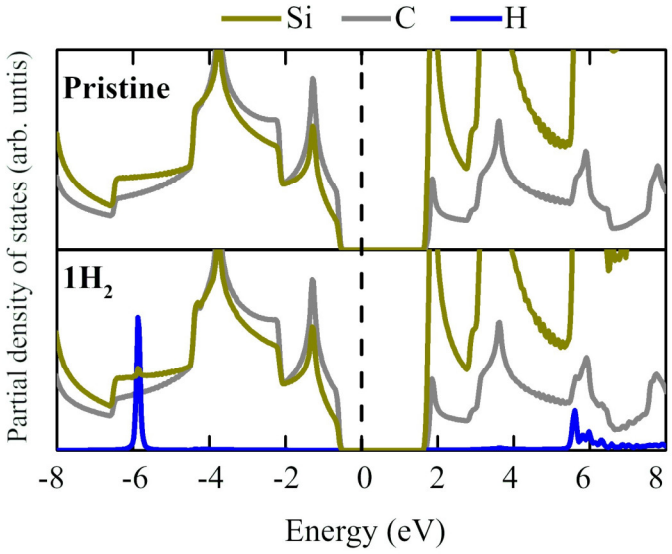

Figure 4. Partial densities of states of the pristine and H_2-adsorbed on pristine SiC monolayer.

Once the preferred site was found, more H_2 molecules were added to see the maximum number of molecules each decorated monolayer can adsorb before the adsorption strength is too weak, or the molecules are too far away from the metal. For this analysis, the adsorption energy was calculated with the following formula:

$$E_a = NE_H + E_{SiC+M} - E_{SiC+M+H}, \quad (3)$$

where E_H is the total energy of a hydrogen molecule, N is the number of hydrogen molecules on the model, E_{SiC+M} is the total energy of the pristine SiC monolayer supercell with a decorating atom, and $E_{SiC+M+H}$ is the total energy of the optimized system of the decorated monolayer supercell with N hydrogen molecules. Table 3 summarizes the results for the calculation with several hydrogen atoms, showing only the results before the hydrogen molecules are too far away or are adsorbed to other H sites with no metal atom.

Table 3. Results for adsorption of N hydrogen molecules on the decorated monolayer: adsorption energies (E_a), average molecule-metal distance (h) and average charge transfer from the molecules to the decorated SiC monolayer (Q_V).

Metal	N	E_a (eV)	h (Å)	Q_V ($\|e\|$)
Li	1	0.26	2.42	0.20
	2	0.29	2.46	0.28
	3	0.29	2.47	0.38
Na	1	0.16	2.74	0.19
	2	0.23	2.76	0.28
	3	0.24	2.76	0.40
	4	0.31	2.78	0.40
K	1	0.13	3.12	0.20
	2	0.22	3.13	0.30
	3	0.22	3.14	0.45
	4	0.22	3.15	0.47
	5	0.20	3.15	0.50
	6	0.20	3.17	0.53
	7	0.19	3.17	0.57
Be	1	0.17	2.19	0.17
Mg	1	0.01	3.11	0
	2	0.12	3.11	0
	3	0.12	3.10	0
	4	0.13	3.10	0
	5	0.13	3.08	0.01
	6	0.13	3.08	0.02
	7	0.13	3.08	0.02
Ca	1	0.02	3.02	0.03
	2	0.13	3.02	0.10
	3	0.13	3.02	0.18
	4	0.15	2.96	0.48
	5	0.16	2.99	0.58
	6	0.16	3.01	0.64
	7	0.16	3.01	0.67

Li- and Be-decorated monolayers have low adsorption capacity, owing probably to their small size. These results agree with other reports on bidimensional SiC (35) and silicene (29). Adsorption on the K-, Mg- and Ca-decorated monolayers is maximum, achieving up to 7 molecules. However, Mg decoration is weak, as shown on Table 1. The results of the Ca-decorated monolayer agree with Song et al. (35), although we found weaker adsorptions. The major capacity with strongest adsorption was found in the case of K, which also showed low electronic charge transfer, which may suggest that, although the molecules are strongly adsorbed on the decorated monolayer, there is no chemical bonding, in other words, the molecules are only physisorbed on the monolayer, and it

will be readily possible to desorb them in order to feed a fuel cell. The H—H bonds were not broken for the H_2 concentrations reported, all of them being 0.79 Å. On Fig. 5 the partial densities of states of the K-decorated monolayer with an increasing number of molecules are plotted. The contribution of H below the Fermi level is centered around -8.5 eV, and these contributions does not modify the Si and C curves as the number of H grows. This evidences the absence of orbital hybridization, and thus chemical bonds, between the H and the atoms of the monolayer.

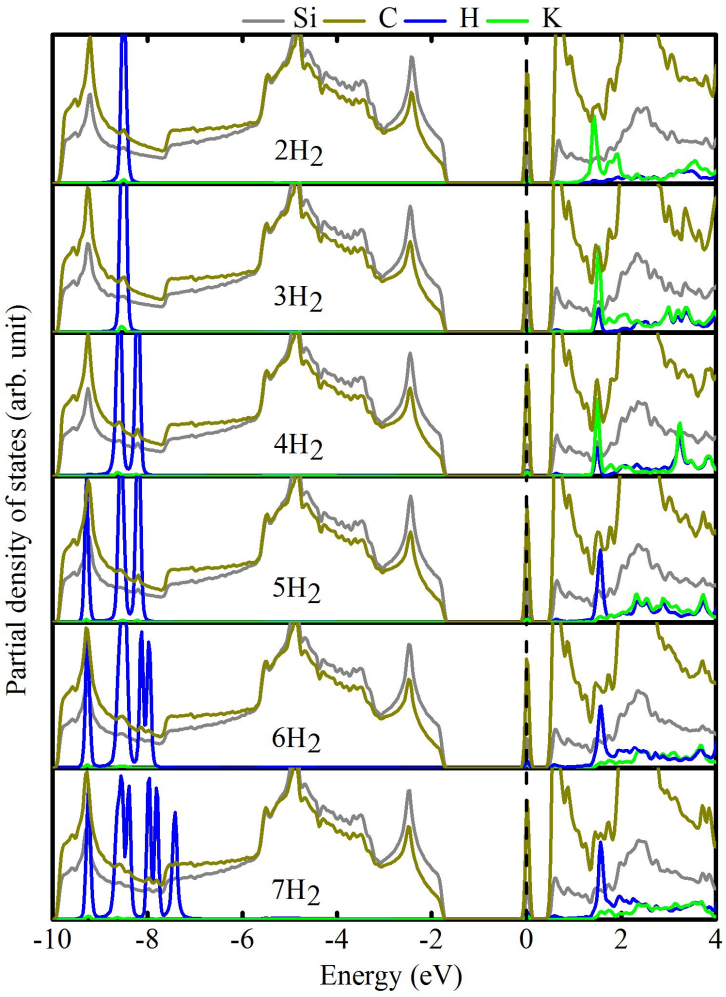

Figure 5. Partial densities of states of the K-decorated SiC monolayer, with an increasing number of H_2 molecules (1 to 7).

4. Conclusions

In this work, the capacity of SiC honeycomb, graphene-like, monolayers decorated with alkali and alkaline-earth metal atoms to physisorb H_2 molecules has been investigated using Density Functional Theory. It was found that alkali and alkaline-earth metals can be chemisorbed on the SiC monolayer, except for Mg, which is physisorbed. The preferred site for the adsorption of metals is the Top (T) site, above a Si atom. While only one H_2 molecule can be adsorbed by the pristine SiC monolayer, the metal-decorated SiC monolayer can adsorb up to 7 molecules (the case of K and Ca adatoms) before the molecules start to be too far from the adatom and adsorb on adjacent H sites. From the perspective of efficient hydrogen storage, the K-decorated SiC monolayer would be the optimal option, as it is the lightest adatom that achieved the largest capacity with reasonably strong adsorption energy. Moreover, it was estimated that only K would avoid clustering over the SiC monolayer. Is important to note that Baierle et al. (34) have recently investigated the adsorption of alkali and alkaline-earth atoms on SiC monolayers, and its possible reaction with a H and O atom. Our results are in excellent agreement with theirs, which were calculated using the VASP code for

DFT, with PAW pseudopotentials and a hybrid exchange-correlation functional. We hope that these results contribute to the ongoing search for ways to engineer materials with desirable properties for clean energy generation and storage.

Acknowledgments

This work was partially supported by multidisciplinary projects IPN-SIP 2018-1937 and 2018-1969, individual project IPN-SIP 2019-5830, and UNAM-PAPIIT IN107717. Computations were performed at the supercomputer Miztli of DGTIC-UNAM (Project LANCAD-UNAM-DGTIC-180), at supercomputer Abacus-I of CINVESTAV-EDOMEX, and at the supercomputer Xiuhcóatl of CINVESTAV (Project LANCAD). F.S. and L.G.A. would like to thank BEIFI-IPN, CONACYT and COFAA-IPN for their financial support. The authors wish to acknowledge the contribution of José A. Galicia for the conception and the early development stages of this work.

References

[1] Ivanov PA, Chelnokov VE. Recent developments in SiC single-crystal electronics. Semicond Sci Technol. 1992;7(7):863–80.

[2] Janzen E, Henry A, Chen WM, Son NT, Monemar B, Sorman E, et al. SiC - A Semiconductor for High-Power , High-Temperature and High- Frequency Devices. Phys Scripta. 1994;54:283–90.

[3] Casady JB, Johnson RW. Status of silicon carbide (SiC) as a wide-bandgap semiconductor for high-temperature applications: A review. Solid State Electron 1996;39(10):1409–22.

[4] Wu R, Zhou K, Yue CY, Wei J, Pan Y. Recent progress in synthesis, properties and potential applications of SiC nanomaterials. Prog Mater Sci 2015;72:1–60.

[5] González I, Trejo A, Calvino M, Miranda A, Salazar F, Carvajal E, M. Cruz-Irisson. Effects of surface and confinement on the optical vibrational modes and dielectric function of 3C porous silicon carbide: An ab-initio study. Phys B Condens Matter 2018;550:420–7.

[6] Tuttle BR, Held NJ, Lam LH, Zhang YY, Pantelides ST. Properties of hydrogenated Nanoporous SiC: An Ab initio study. J Nanomater. 2017;2017:4705734.

[7] Calvino M, Trejo A, Crisóstomo MC, Iturrios MI, Carvajal E, Cruz-Irisson M. Modeling the effects of Si-X (X = F, Cl) bonds on the chemical and electronic properties of Si-surface terminated porous 3C-SiC. Theor Chem Acc. 2016;135(4):104.

[8] Tabtimsai C, Ruangpornvisuti V, Tontapha S, Wanno B. A DFT investigation on group 8B transition metal-doped silicon carbide nanotubes for hydrogen storage application. Appl Surf Sci 2018;439:494–505.

[9] Li YJ, Li SL, Gong P, Li YL, Fang XY, Jia YH, Cao MS. Inhibition of quantum size effects from surface dangling bonds: The first principles study on different morphology SiC nanowires. Phys B Condens Matter 2018;539(January):72–7.

[10] Cuevas JL, de Santiago F, Ramírez J, Trejo A, Miranda Á, Pérez LA, Cruz-Irisson M. First principles band gap engineering of [1 1 0] oriented 3C-SiC nanowires. Comput Mater Sci. 2018;142:268–76.

[11] Miranda A, Cruz-Irisson M, Perez LA. Controlling stability and electronic properties of small-diameter SiC nanowires by fluorination. Int J Nanotechnol. 2015;12(3–4):218–25.

[12] Zhao L, Chen S, Wang L, Gao F, Yao X, Yang W. Large-scale fabrication of free-standing and transparent SiC nanohole array with tailored structures. Ceram Int. 2018;44(6):7280–5.

[13] Li X, Chen S, Ying P, Gao F, Liu Q, Shang M, Yang W. A giant negative piezoresistance effect in 3*C*-SiC nanowires with B dopants. J Mater Chem C. 2016;4(27):6466–72.

[14] Dinh T, Phan HP, Nguyen TK, Balakrishnan V, Cheng HH, Hold L, Lacopi A, Nguyen N-T, Dao DV. Unintentionally Doped Epitaxial 3C-SiC(111) Nanothin Film as Material for Highly

Sensitive Thermal Sensors at High Temperatures. IEEE Electron Device Lett. 2018;39(4):580–3.

[15] Lin SS. Light-emitting two-dimensional ultrathin silicon carbide. J Phys Chem C. 2012;116(6):3951–5.

[16] Frisenda R, Molina-Mendoza AJ, Mueller T, Castellanos-Gomez A, Van Der Zant HSJ. Atomically thin p-n junctions based on two-dimensional materials. Chem Soc Rev. 2018;47(9):3339–58.

[17] Liu X, Ma T, Pinna N, Zhang J. Two-Dimensional Nanostructured Materials for Gas Sensing. Adv Funct Mater. 2017;27(37):1–30.

[18] Choi SJ, Kim ID. Recent Developments in 2D Nanomaterials for Chemiresistive-Type Gas Sensors. Electron Mater Lett. 2018;14(3):221-60.

[19] Feng YP, Shen L, Yang M, Wang A, Zeng M, Wu Q, Chintalapati S, Chang C-R. Prospects of spintronics based on 2D materials. Wiley Interdiscip Rev Comput Mol Sci. 2017;7(5):e1313.

[20] Shi L, Zhao T. Recent advances in inorganic 2D materials and their applications in lithium and sodium batteries. J Mater Chem A. 2017;5(8):3735–58.

[21] Bekaroglu E, Topsakal M, Cahangirov S, Ciraci S. First-principles study of defects and adatoms in silicon carbide honeycomb structures. Phys Rev B - Condens Matter Mater Phys. 2010;81(7):1–9.

[22] Chabi S, Chang H, Xia Y, Zhu Y. From graphene to silicon carbide: Ultrathin silicon carbide flakes. Nanotechnology. 2016;27(7):075602.

[23] Susi T, Skákalová V, Mittelberger A, Kotrusz P, Hulman M, Pennycook TJ, . Computational insights and the observation of SiC nanograin assembly: Towards 2D silicon carbide. Sci Rep. 2017;7(1):4399.

[24] Gaudernack B, Lynum S. Hydrogen from natural gas without release of CO_2 to the atmosphere. Int J Hydrogen Energy. 1998;23(12):1087–93.

[25] Niaz S, Manzoor T, Pandith AH. Hydrogen storage: Materials, methods and perspectives. Renew Sustain Energy Rev. 2015;50:457–69.

[26] Liu T, Ding J, Su Z, Wei G. Porous two-dimensional materials for energy applications: Innovations and challenges. Mater Today Energy 2017;6:79–95.

[27] Yu X, Tang Z, Sun D, Ouyang L, Zhu M. Recent advances and remaining challenges of nanostructured materials for hydrogen storage applications. Prog Mater Sci. 2017;88:1–48.

[28] Honarpazhouh Y, Astaraei FR, Naderi HR, Tavakoli O. Electrochemical hydrogen storage in Pd-coated porous silicon/graphene oxide. Int J Hydrogen Energy. 2016;41(28):12175–82.

[29] Wang Y, Zheng R, Gao H, Zhang J, Xu B, Sun Q, Jia Y. Metal adatoms-decorated silicene as hydrogen storage media. Int J Hydrogen Energy. 2014;39(26):14027–32.

[30] Du A, Zhu Z, Smith SC. Multifunctional Porous Graphene for Nanoelectronics and Hydrogen Storage: New Properties Revealed by First Principle Calculations. J Am Chem Soc. 2010;132(9):2876–7.

[31] Sun Q, Wang Q, Jena P, Kawazoe Y. Clustering of Ti on a C_{60} Surface and Its Effect on Hydrogen Storage. J Am Chem Soc. 2005;127(42):14582–3.

[32] Krasnov PO, Ding F, Singh AK, Yakobson BI. Clustering of Sc on SWNT and reduction of hydrogen uptake: Ab-initio all-electron calculations. J Phys Chem C. 2007;111(49):17977–80.

[33] Chakraborty B, Modak P, Banerjee S. Hydrogen storage in yttrium-decorated single walled carbon nanotube. J Phys Chem C. 2012;116(42):22502–8.

[34] Baierle RJ, Rupp CJ, Anversa J. Alkali (Li, K and Na) and alkali-earth (Be, Ca and Mg) adatoms on SiC single layer. Appl Surf Sci 2018;435:338–45.

[35] Song N, Wang Y, Zheng Y, Zhang J, Xu B, Sun Q, Jia Y. New template for Li and Ca decoration and hydrogen adsorption on graphene-like SiC: A first-principles study. Comput Mater Sci 2015;99:150–5.

[36] Pantha N, Belbase K, Adhikari NP. First-principles study of the interaction of hydrogen molecular on Na-adsorbed graphene. Appl Nanosci. 2015;5(4):393–402.

[37] Hohenberg P, Kohn W. Inhomogeneous Electron Gas. Phys Rev 1964;136(3B):B864–71.

[38] Kohn W, Sham LJ. Self-Consistent Equations Including Exchange and Correlation Effects. Phys Rev 1965;140(4A):A1133–8.

[39] Soler JM, Artacho E, Gale JD, García A, Junquera J, Ordejón P, Sánchez-Portal D. The SIESTA method for *ab initio* order-*N* materials simulation. J Phys Condens Matter 2002;14(11):2745.

[40] Perdew JP, Burke K, Ernzerhof M. Generalized Gradient Approximation Made Simple. Phys Rev Lett 1996 Oct 28;77(18):3865–8.

[41] Artacho E, Sánchez-Portal D, Ordejón P, García A, Soler JM. Linear-Scaling ab-initio Calculations for Large and Complex Systems. Phys status solidi 1999;215(1):809–17.

[42] Junquera J, Paz Ó, Sánchez-Portal D, Artacho E. Numerical atomic orbitals for linear-scaling calculations. Phys Rev B 2001;64(23):235111.

[43] Troullier N, Martins JL. Efficient pseudopotentials for plane-wave calculations. Phys Rev B 1991;43(3):1993–2006.

[44] Kleinman L, Bylander DM. Efficacious Form for Model Pseudopotentials. Phys Rev Lett 1982;48(20):1425–8.

[45] Monkhorst HJ, Pack JD. Special points for Brillouin-zone integrations. Phys Rev B. 1976;13(12):5188–92.

[46] Fonseca Guerra C, Handgraaf J-W, Baerends EJ, Bickelhaupt FM. Voronoi deformation density (VDD) charges: Assessment of the Mulliken, Bader, Hirshfeld, Weinhold, and VDD methods for charge analysis. J Comput Chem. 2004;25(2):189–210.

[47] Oura K, Katayama M, Zotov AV, Lifshits VG, Saranin AA. Surface Science. Springer; 2003.

[48] Kittel C. Introduction to Solid State Physics. Wiley; 2004.

Meguellati Farouk, 3637
Melián-Martel Noemi, 3697
Melka Bartlomiej, 4723
Mendecka Barbara, 3483, 4043, 4625
Menezes Marcela, 2067, 4661
Merchán Corral Rosa, 479, 1079
Mesfun Sennai, 1519
Micali Francesco, 4625
Miccio Francesco, 3599
Middelhauve Luise, 377
Miecznik Maciej, 4387, 4409
Mihailiasa Manuela, 4589
Mika Łukasz, 3137, 4761
Mikielewicz Dariusz, 2699, 2751, 3237
Milewski Jarosław, 411, 2913, 4781
Milivojevic Sanja, 2973
Milutinović Biljana, 3769
Miranda Álvaro, 4297, 4311
Miranda Lira Lucas, 1771
Mitukiewicz Grzegorz, 3249
Mlonka-Mędrala Agata, 4107
Moździerz Marcin, 2983
Modesto Marcelo, 77, 465, 2255
Mohamed Omer-Elfarouk E., 453
Momčilović Ana, 3769
Monaghan Rory, 1113
Monforti Ferrario Andrea, 3347
Montero Eduardo, 51, 203
Moradi Ramin, 3347
Morais Pedro, 77, 465, 2255
Moret Stefano, 761
Morosuk Tatiana, 4445
Mossberg Johanna, 1921
Motas Justina, 4557
Motylinski Konrad, 2649
Mouaky Ammar, 609
Mullen David, 2201
Munoz-Rujas Natalia, 51
Musiał Dorota, 4133
Mustafa Ibrahim, 3875

Najjaran Ahmad, 1055
Nakashima Rafael, 1687
Nascimento Silva Fernanda, 2453
Nastro Rosa Anna, 3833
Nazir Shareq Mohd, 635
Nebra Silvia, 1781, 2379, 2393
Nedelcu Dumitru, 4557
Nemś Artur, 2569
Nemś Magdalena, 2569, 3261
Nemer Maroun, 189, 275
Nesiadis Athanasios, 3555
Neto José, 3521
Neveu Pierre, 2555, 3065
Niedźwiecki Łukasz, 4107
Niederdränk Anne, 339
Nijs Wouter, 2135
Nikolopoulos Aristeidis, 3645, 3659
Nikolopoulos Nikos, 3555, 3645, 3659
Noury Agnieszka, 3249
Noussan Michel, 787
Nova-Rincón Arley, 595
Novazzi Luis Fernando, 1771
Nowak Andrzej, 4493
Nowak Wojciech, 1325, 2531, 3137

O'rourke Fergal, 2075
O. S. Medeiros Giulia, 1579
Ogata Keito, 1235
Oikawa Ryo, 887
Oláhné Groma Veronika, 4223
Oladipo Oluwafunmilola, 3261
Oliveira Guilherme, 3521
Oliveira Junior Silvio, 1687, 2453, 2781, 3007, 3077
Olympios Andreas, 1043, 1055
Ommen Torben, 2323
Ong Chun Wei, 925
Onishi Takeshi, 2187
Oonishi Takayuki, 1843
Orehounig Kristina, 775
Orlande Helcio, 3381
Orozco L Carlos A, 4283
Ortego Abel, 3715
Ortiz Carlos, 4323
Orujov Farid, 4555
Osseweijer Patricia, 1163
Otsubo Kensuke, 1843
Oyekale Joseph, 999
Oyewunmi Oyeniyi, 1759

Pérez Álvaro, 1015
Pérez Eduardo, 1185
Pérez Luis, 4297, 4311
Périer-Muzet Maxime, 2555
Padey Pierryves, 3101
Pahud Daniel, 3101
Pajączek Krzysztof, 4707
Pająk Leszek, 4387, 4409
Pająk Marcin, 419
Pajdak Anna, 4579, 4583
Palacios Jose, 2283, 3791, 3803, 4539
Palacios-Bereche Milagros, 1781
Palacios-Bereche Reynaldo, 1067, 1781
Palacz Michał, 3391